HHS Public Access

Author manuscript

Magn Reson Med. Author manuscript; available in PMC 2016 June 01.

Published in final edited form as:

Magn Reson Med. 2010 May ; 63(5): 1383–1390. doi:10.1002/mrm.22313.

Magnetic Nanoparticles for Imaging Dendritic Cells

Saho Kobukai[1], **Richard Baheza**[1], **Jared G. Cobb**[1], **Jack Virostko**[1], **Jingping Xie**[1], **Amelie Gillman**[1], **Dmitry Koktysh**[2], **Denny Kerns**[3], **Mark Does**[1,4], **John C. Gore**[1,4], and **Wellington Pham**[1,4,*]

[1]Vanderbilt University, Institute of Imaging Science, Nashville, Tennessee, USA

[2]Department of Chemistry, Vanderbilt Institute of Nanoscale Science and Engineering, Nashville, Tennessee, USA

[3]Vanderbilt Electron Microscope Resource, Nashville, Tennessee, USA

[4]Department of Biomedical Engineering, Nashville, Tennessee, USA

Abstract

We report the development of superparamagnetic iron oxide (SPIOs) nanoparticles and investigate the migration of SPIO-labeled dendritic cells (DCs) in a syngeneic mouse model using magnetic resonance (MR) imaging. The size of the dextran-coated SPIO is roughly 30 nm, and the DCs are capable of independent uptake of these particles, although not at levels comparable to particle uptake in the presence of a transfecting reagent. On average, with the assistance of polylysine, the particles were efficiently delivered inside DCs within one hour of incubation. The SPIO particles occupy approximately 0.35% of cell surface and are equivalent to 34.6 pg of iron per cell. In vivo imaging demonstrated that the labeled cells migrated from the injection site in the footpad to the corresponding popliteal lymph node. The homing of labeled cells in the lymph nodes resulted in a signal drop of up to 79%. Furthermore, labeling DCs with SPIO particles did not compromise cell function, we demonstrated that SPIO-enhanced MR imaging can be used to track the migration of DCs effectively in vivo. Magn Reson Med 63:1383–1390, 2010.

Keywords

nanoparticles; dendritic cells; T2-weighted imaging; lymph nodes; immunotherapy

Dendritic cells (DCs) play key roles in the induction and modulation of antigen-specific immune responses against bacteria, viruses, allergens, and tumor antigens ([1–3]). They serve as essential components of the immune system in triggering immune reactions, thereby making them promising tools for immunotherapy ([4,5]). Despite its appeal, however, several limitations exist in the use of antigen-pulsed DCs in cell therapy. A key question in DC-based therapy that has yet to be consistently answered is the cellular fate of the DCs after injection. Migration from the injection site to the secondary lymphoid tissues is critical for the DCs to accomplish their function as antigen-presenting cells ([6]). Regardless of the

*Correspondence to: Wellington Pham, Vanderbilt University, Institute of Imaging Science, 1161 21st Avenue South, AA. 1105 MCN, Nashville, TN 37232-2310. ; Email: wellington.pham@vanderbilt.edu

ability to generate potent DCs in vitro, they remain ineffective as a means of accomplishing immunotherapy unless migration to the regional lymph node (LN) can be achieved ([7]). These drawbacks of DC-based therapy have been subjected to close scrutiny during the past few years.

Recently, we developed a technique for optically imaging the global distribution of DCs in a whole mouse ([8]). While it is increasingly recognized that optical imaging of DCs plays an important role in deciphering the kinetic and specific interactions in the microenvironment within the lymphoid tissue, it is undoubtedly true that MRI could serve as an ideal modality for detecting the migration of DCs into the LNs due to its high soft tissue contrast and spatial resolution. Toward this approach, Ahrens et al. ([9]) developed a method for labeling DCs with superparamagnetic iron oxide (SPIO) to monitor cell trafficking in vivo. The technique employed a receptor-mediated endocytosis mechanism, where SPIO were conjugated to anti-CD11c monoclonal antibodies. In another work, de Vries et al. ([10]) demonstrated that autologous DCs can uptake ferumoxide directly without using a targeted delivery approach, albeit with longer incubation time. In the present study, we used a different approach and utilized polylysine (PL) as a transfecting reagent to shuttle the in-house-developed SPIO into DCs. A detailed study showed that in the presence of a transfecting reagent, the nanoparticles were effectively delivered into DCs without any registered cytotoxic effect. We further provide evidence that demonstrates that it is possible to track the migration of a small population of DCs noninvasively using MRI after adaptively transferring the cells into a syngeneic mouse model.

MATERIALS AND METHODS

Adult C57BL/6 mice were obtained from the Jackson Laboratory (Bar Harbor, ME) and bred in house. Animal experiments were carried out per the guidelines provided by the Vanderbilt University Institutional Animal Care and Use Committee and the National Institutes of Health Guide for the Care and Use of Laboratory Animals.

Developing SPIO Nanoparticles

Dextran-coated iron oxide nanoparticles were fabricated in our laboratory, using a reported protocol, with some modifications ([11,12]). In brief, a saturated mixture of dextran and ferric chloride was coalesced with a ferrous chloride solution at room temperature, followed by elevating the pH to 10 via dropwise addition of an ammonium hydroxide solution. The resulting solution was stirred for several hours.

The synthesized particles were separated from the starting materials, using deionized water, and then dialyzed into buffer representing the normal physiologic concentrations of sodium citrate and sodium chloride.

The concentration of iron in the solution was determined by inductively coupled plasma mass spectrometry. To obtain the designed concentration of SPIO nanoparticles for analysis, a stock solution of SPIO particles was diluted 1:10,000 in 1% nitric acid solution. Each experiment was performed in duplicate.

Measuring the Size and Shape of the Magnetite Core

The size and shape of the magnetite cores were determined by high-resolution transmission electron microscopy (TEM), using a Philips CM12 microscope (FEI, Hillsboro, OR) with an accelerating voltage of 80 kV. Both the particle size distribution and the size of any aggregates were evaluated. The samples were prepared by adding a ~40 μL drop of a suspension of the particles (1 mg/mL) onto a formvar (polyvinyl formal)-coated copper grid (3mm in diameter). Any excess water was quickly wicked off so that the particles would adhere to the plastic support via electric charge. Following this step, we added to the grid a drop of aqueous stain (phosphotungstate), surrounding the particles without penetrating them. The TEM images were viewed as a negative contrast.

The hydrodynamic diameter of the SPIO particles was determined through dynamic light scattering on a Zetasizer Nano ZS (Malvern Instruments, UK). Zetasizer incorporates noninvasive backscatter optics and a 633-nm laser. The optical density of the SPIO particles solution was 0.18 at 633 nm. The particle size was measured at 25°C, and data were collected after 12 consecutive measurements.

MR Relaxivity Measurement

Colloidal suspensions of the SPIO particles were diluted with deionized water to concentrations of 0.717 mM, 1.43 mM, 3.59 mM, and 7.171 mM. These samples, along with a deionized water control solution containing no SPIO particles, were placed in 5mm-diameter NMR tubes. The NMR tubes were positioned in the isocenter of a 25mm-diameter Litz coil (Doty Scientific, Columbia, SC) for radiofrequency transmission and signal reception. Imaging was performed at 200 MHz on a 4.7-T horizontal-bore magnet equipped with a Varian Inova console (Varian Inc., Palo Alto, CA).

Longitudinal relaxation rate (R_1) was determined using a series of T_1-weighted gradient echo images acquired with different repetition times (pulse repetition time [TR] = 100 ms to 550 ms). Other imaging parameters were echo time (TE) = 3.64 ms, flip angle = 20°, field of view = 17.1 × 19.2mm, and matrix size = 128 × 128. The average signal intensity in each NMR tube was used to determine the R_1 through nonlinear least squares fit, using MATLAB.

The transverse relaxation rate (R_2) was determined using a single-slice, multiecho pulse sequence with 32 echoes at TE = 8.5 ms. Other imaging parameters were TR = 1200 ms, field of view = 15 × 15mm, and matrix size = 32 × 32. The average signal intensity in each NMR tube was used to determine the R_2 by conducting a linear fit using MATLAB's polyfit function between TE and log (signal) corrected for Rician noise.

MRI

Phantom and in vivo MRI was performed on a 4.7-T Varian Inova scanner. For the former, labeled DCs were embedded in 6% gelatin, and MRI was performed by using a T_2-weighted spin-echo (TR = 5 sec, TE arrayed with values of 15, 55, 95, 135, 175, and 215 ms, field of view = 40 × 40mm^2, acquisition matrix = 256 × 256, and slice thickness = 1.0 mm, and gap = 0 mm). In vivo imaging used T_2-weighted imaging, with a spin echo multislice using a

respiration-gated generating TR variable from 2 to 3 sec, field of view = 35 × 35mm, TE = 10 ms, matrix size = 256 × 256, and slice thickness = 0.5mm, which resulted in a voxel time of $0.137 \times 0.137 \times 0.5\text{mm}^3$.

MRI of mice ($n = 10$) was performed before and 24 h after injection of 4000 and 1.0×10^6 SPIO-labeled DCs (each 30 μL) into each hind foot pad.

Image Processing

Signal intensity was measured in all animals for the popliteal and inguinal LNs (both sides), and also background tissues such as fat and muscle, for at least three regions of interest per measurement of all sequences. The standard deviation (SD) of the signal within the LNs was recorded as a noise.

The contrast-to-noise ratio was measured for each region of interest (ROI), using the formula contrast-to-noise ratio = $(\text{ROI}_{\text{fat}} - \text{ROI}_{\text{LN}})/\text{SD}_{\text{noise}}$. Signal-to-noise ratios were measured for the LNs according to the relation of signal-to-noise ratio = $\text{SI}_{\text{org}}/\text{SD}$, where SI_{org} represents the signal intensity of the organ and SD is the SD of background noise. The contrast generated by T_2-mediated signal was quantified using ImageJ software (National Institutes of Health, Bethesda, MD).

Isolation of DCs

DCs were isolated from mouse bone marrow, as described, with slight modifications ([8,13]). Briefly, bone marrow cells in the femurs and tibias of mice were flushed out with RPMI medium (Invitrogen, Carlsbad, CA), using a 1 mL syringe incorporating a 27 gauge needle (BD Biosciences, San Jose, CA). The cells were collected into a 50 mL conical tube after being passed through a 40 μm pore sized nylon mesh cell strainer (BD Biosciences). The red cells were removed from the bone marrow cells with 3 min of incubation time in 0.83% ammonium chloride at room temperature, followed by two washes with RPMI medium. The remaining bone marrow cells were counted and cultured in a 100mm cell culture dish (BD Biosciences) at a density of $3–5 \times 10^6$ cells per dish. The medium used for DC preparation was supplemented with 50 mM of 2-mercaptoethanol, 100-mM sodium pyruvate (Invitrogen), 100 U/mL penicillin, 100 mg/mL streptomycin (Invitrogen), 200 U/mL recombinant murine granulocyte macrophage-colony stimulating factor (GM-CSF), and 50 U/mL interleukin 4 (IL-4) (both from PeproTech, Rocky Hill, NJ). New medium containing GM-CSF and IL-4 was added to each plate on day 3 of culture. On day 6, half of the medium in each dish was replaced with new medium supplemented with cytokines. On day 8, weakly attached cells were collected and used for experiments as immature DCs.

Cell Labeling and Staining

Magnetic cell labeling and determination of intracellular uptake were conducted by first incubating detached immature DCs, at a concentration of 5×10^6 cells/mL, with SPIO particles to a final concentration of 1 mg/mL for 1 h at room temperature, with or without the addition of 20 μg/mL PL. Following incubation with the SPIO particles, the DCs were washed three times with phosphate-buffered saline to eliminate any extracellular SPIO.

The efficiency of labeling and intracellular uptake by the DCs was confirmed by Prussian blue staining and electron microscopy. For Prussian blue staining, the SPIO-loaded DCs were immobilized to a glass slide by cytospin. Briefly, one aliquot of 100 μL of DCs (10^6 cells/mL) in medium with 1% serum was pelleted onto each slide. The slides were dried at room temperature and fixed with 4% paraformaldehyde for 10 min. The samples were then stained with freshly mixed 10% hydrochloric acid and 5% potassium ferrocyanide solution for 20 min. After three washes with water, the slides were counterstained with 0.1% nuclear fast red for 5 min. After a rinse with water, the slides were dried and examined under a microscope.

Prussian blue staining of the popliteal LNs was performed according to a reported procedure ([14]). The LNs were soaked in 10% formalin for 5 h, followed by 70% ethanol overnight. Then, the samples were embedded in paraffin and sliced. After deparaffinization, the slides were placed in a mixture of 2% potassium ferrocyanide and 2% hydrochloric acid for 20 min at 60°C. Following three washes with distilled water, the slides were counterstained with 0.1% nuclear fast red for 5 min. Finally, the slides were dehydrated in 95% ethanol and mounted with synthetic resin.

Cell Surface Phenotyping

The phenotype of DCs, pre- and postlabeling with SPIO particles, was analyzed using a BD LSRII flow cytometer (BD Biosciences) and FlowJo software (Tree Star, Ashland, OR) at the Vanderbilt Flow Cytometry Core laboratory. The cells were pretreated with affinity-purified anti-mouse CD16/CD32 monoclonal antibody (eBio-science, San Diego, CA) to block any nonspecific antibody binding. For each set of staining groups, 1.0×10^6 cells were incubated with monoclonal antibodies on ice in 1% fetal calf serum containing phosphate-buffered saline for 30 min, washed twice with phosphate-buffered saline, and then analyzed. The monoclonal antibodies used for the DC surface staining were as follows: fluorescein isothiocyanate anti-mouse major histocompatibility complex (MHC) class I (28-8-6; R&D Systems, Minneapolis, MN), fluorescein isothiocyanate anti-mouse MHC class II (eBioscience), R-phycoerythrin-Cy7 anti-mouse CD11c (Integrin aX, p150/90; eBioscience), phycoerythrin anti-mouse CCR7 (CD197, EBI-1; eBioscience), allophycocyanin (antigen-presenting cell) anti-mouse CD80 (B7-1; eBioscience), and antigen-presenting cell anti-mouse CD86 (B7-2; eBioscience). Unstained DCs or isotypic control antibodies were used as negative controls.

MATLAB Program for Analysis of SPIO Occupancy Inside the DCs

The analysis incorporated several operations performed on a cell image via a built-in function in MATLAB used primarily for interactively specifying ROIs. Manual tasks included outlining the cell body, associating a length of contiguous pixels with the spatial dimensions noted in the image, specifying a subset of interest within the cell, and selecting an ROI within that subset. The program calculated the mean and SD of the pixel intensity values within the ROI and then identified all the pixels within the selected image subset that displayed intensity values within the range of the ROI mean intensity, ± 3 SDs. Following this automatic thresholding, the classified subset was then visually inspected, and ROIs were manually drawn to specify what appeared to be spurious inclusions (e.g., lack of multipixel

continuity indicative of selections too small to be particles, portions of the cell that were better ascribed to nonparticle components) in the classification process. The application then retracted these latter ROIs from the classification and calculated the SPIO occupancy percentage based on the number of pixels in the cell body, the number of pixels meeting the standards for admission into the class of particles, and the dimensions of each pixel.

Imaging the Iron Content Inside DCs Using TEM

The SPIO-labeled DCs were pelleted and then fixed with 2.5% glutaraldehyde and 0.1-M sodium cacodylate for 1 h. The sample was then rinsed with sodium cacodylate (twice, 5 min for each wash), followed by a second fixing with 1% osmium tetroxide for 1 h. The sample was rinsed several times with 50%, 70%, 95%, and 100% ethanol and then with 50% and 100% propylene oxide. The samples were then dehydrated and filtered onto an Epon 812 resin-coated copper grid. The sections were imaged on a Philips CM 12 microscope.

Histology Analysis of Migration to the LNs

Immunohistochemistry of the LN sections was performed as described previously ([8]). Briefly, after completion of the in vivo imaging experiment, the animals were sacrificed and the popliteal LNs were excised and cut in half for either Prussian blue staining or immunohistology. Prussian blue staining for the popliteal LNs was performed as described above. For the CD11c immunohistochemistry of DCs in the LN, the samples were first snap frozen in liquid nitrogen. Five-micrometer sections of the frozen LN tissues were then placed on charged slides. The slides were then treated with hydrogen peroxide to neutralize any endogenous peroxidases and treated with a UV block (Lab Vision, Fremont, CA) for 5 min to block any nonspecific staining prior to primary antibody addition. Then, the slides were incubated with affinity-purified hamster anti-CD11c antibody (eBioscience), diluted 1:200 for 60 min, followed by treatment with the Vectastain ABC Elite system (Vector Laboratories, Burlingame, CA) and 3,3′-diaminobenzidine (Dako, Carpinteria, CA) to produce localized, visible staining. Finally, the slides were counterstained with Fast Green (Dako). All sections were visualized using a Zeiss Axioskop 40 microscope (Carl Zeiss MicroImaging, Thornwood, NY) equipped with AxioCam (Carl Zeiss MicroImaging) for digital images with a 40× objective lens.

Statistical Analysis

Data were expressed as means ± SD. The statistical significance of the differences between sample means was determined by Student's t test for independent samples, and the results were considered significant when $P < 0.05$ with GraphPad Prism software.

RESULTS

Physical Properties of SPIO

The iron cores of the developed SPIO particles are uniform in size and shape (Fig. 1). The average spherical size of the core is approximately 9 ± 2.4 nm in diameter, as calculated from TEM images. After coating with dextran, the whole dextran-magnetite complex has a mean hydrodynamic diameter of approximately 30 nm. The T_1 and T_2 relaxation times were measured at 4.7 T, and the relaxation constants were determined from the slope of the linear

plots of $1/T_1$ and $1/T_2$ versus iron concentrations between 1.0 and 4 mM. The developed SPIO particles appear to have a high R_2/R_1 ratio (R_1 = 0.05 S^{-1} mM^{-1}; R_2 = 0.3 S^{-1} mM^{-1}), which makes them suitable for T_2-weighted imaging.

Labeling DCs With SPIO

PL effectively mediated the internalization of the SPIO particles inside immature DCs within 1 h of incubation, specifically for 4000 cells in culture media containing 1 mg/mL SPIO particles. The labeling efficiency was apparent when the cells turned from opaque to brown, and intracellular residence of the particles was validated by Prussian blue staining. The blue dots indicated the presence of iron inside the DCs (Fig. 2). As expected, MRI of the labeled cells in a gelatin phantom tube experienced a remarkable drop in signal intensity ($P < 0.0001$). In the absence of PL, however, incubation of more than double the number of cells with the same concentration of SPIO particles did not show favorable uptake of the nanoparticles, as observed with the Prussian blue staining. Nevertheless, a modest signal decrease was observed. Taken together, DCs are capable of internalizing some SPIO particles without assistance from PL treatment. However, the striking difference in the amount of particle uptake in the presence of transfecting agents is quite compelling, given that this does not compromise cell viability.

Phenotypical Expression of Labeled DCs

Labeling DCs with SPIO particles did not affect their phenotypical expression of surface receptors or maturation. In the flow cytometry assay, isolated and immature DCs were split into two batches. We labeled one these with 1 mg/mL of SPIO particles and used the other as a control. The labeled and unlabeled DCs were then divided into two batches; one of them was stained with secondary antibodies specific to each of the known surface molecules, while the other was used for isotype controls. The left histograms in Fig. 3 represent the unstained controls of either labeled or unlabeled DCs, and the right and shifted histograms represent labeled and unlabeled DCs, which were stained with the corresponding antibodies. The DC population was gated by side and forward scattering to exclude other cells. The surface phenotype of SPIO-labeled DCs exhibited typical expression patterns typical for CD11c, MHC-I, MHC-II, costimulatory molecules of CD80, CD86, and chemokine receptor type 7 molecules CCR7.

MRI of Cell Migration

For this study, two different populations of labeled DCs were adaptively transferred to a syngeneic mouse (n = 10). The purpose was to test the detection limit for the number of DCs using MRI. The mice received either 4000 or 1.0×10^6 SPIO-labeled DCs by injection in the left or right foot pads. Both cell populations were incubated with 1 mg/mL SPIO particles for 1 h prior to injection, and the LNs were scanned before and 24 h after injection. Figure 6 shows that the axial LNs are clearly visible in MR images due their contrast with the surrounding fat pad. In order to generate brighter LNs that can be used to distinguish the labeled DCs, we adjusted the TR from 1 to 2 sec. By using the described parameter, we can distinguish the LNs embedded inside the fat pad. The characteristically bright signal and specific shape of the fat in both inguinal and popliteal LNs served as excellent guidance for

locating the LNs. In general, we found that the signal-to-noise ratio of the LNs was 10 (n = 10) and the contrast-to-noise ratio of the fat LNs was 7.5 (n = 10).

The MR images indicated the migration of DCs into both the left and right popliteal LNs. The signal intensity of right popliteal LN was reduced by 79.4% at 24 h post-injection, while this value was 55.8% for the left popliteal LN. We did not observe any signal change in the inguinal LNs by 24 h postinjection, indicating that the injected DCs could migrate to the first draining LNs. However, there was no evidence of movement from the first homing to the next LN.

DISCUSSION

The long-term objective of our work is to investigate a noninvasive method for tracking cell migration, with the potential for clinical application. To that end, we aimed to develop magnetic nanoparticles for MRI. The particles are very uniform in size and shape and are well dispersed. We did not observe any level of aggregation, precipitation, or deterioration during the course of this study (approximately 2 years). Using current chemistry, the concentration of the SPIO particles could be made as high as 12–15 mg/mL.

Previous work from our group demonstrated that, despite being considered antigen-presenting cells, DCs do not uptake fluorescence probes to any extent ([8]). Therefore, a delivery molecule was developed for transporting the probe into the DCs. In this work, we observed that immature DCs can phagocytose our newly developed SPIO nanoparticles, albeit at a significantly slow rate. Figure 2 shows that the signal change of the phantom tube containing 10,000 DCs incubated with SPIO particles was much smaller when compared to that of the other tube containing 4000 DCs that were incubated with SPIO particles in the presence of PL (Fig. 2a). Prussian blue staining also showed the infinitesimal uptake in this non-PL-mediated group (Fig. 2b, left). This was further confirmed by MRI, with which a much longer scanning time was required to depict a signal drop (Fig. 2a). In contrast, the PL facilitated the uptake of the SPIO particles by the DCs (Fig. 2a,b, right); within 1 h of incubation, the signal intensity dropped 97%, with a TE of 15 ms ($P < 0.0001$) (Fig. 2c). The PL-free group needed up to 215 ms to visualize a 60% drop in signal ($P < 0.0002$).

We also observed that the DCs became unhealthy when they were exposed to high concentrations of SPIO (>5 mg/mL) in the presence of PL (data not shown), and we therefore maintained a concentration of 1.0 mg/mL SPIO throughout the experiment. Phagocytes differ from other cells in that they undergo a dynamic phenotypical transformation that is associated with their function as antigen-presenting cells. Any toxicity to the cells due to the nanoparticles will compromise this phenotypical transformation, which is manifested by the expression of certain surface receptors on the DCs. These surface receptors are important for communicating the signal that then triggers the activation and proliferation of T cells. Antigens are first presented through the MHC, which is followed by interactions between the CD28 on T cells with costimulatory molecules, B7-1 (CD80) and B7-2 (CD86) of the DCs. Flow cytometric analysis, which was performed to determine whether the SPIO-labeled DCs were still healthy, showed that the SPIO labeling procedure did not affect either the phenotypical expression or maturation of the DCs (Fig. 3). The level

of murine DC surface markers (CD11c), costimulatory molecules (CD80, CD86), chemokine receptors (CCR7), and MHC (class I/II) between the unlabeled control DCs and SPIO-labeled cells was comparable.

In addition to using Prussian blue staining to confirm the internalization of the SPIO particles by the DCs, the process was further validated using TEM (Fig. 4). We observed that the SPIO particles were initially engulfed by DCs into the endocytic vesicles close to the intracellular membrane, followed by transport farther inward toward the cytoplasm. The particles were confined to the vesicles, and this observation was in agreement with previous work reported by Baumjohannn et al. ([15]), although the transfecting agent used in their works is different. The internalization of the SPIO nanoparticles in the vesicles likely prevents any subsequent interference with normal intracellular functions. From an imaging standpoint, the directed accumulation of SPIO particles in the endocytic vesicles concomitantly brings these particles together into a cluster setting, thus making the small SPIO particles seem larger. In theory, this DC-mediated aggregation would enhance the signal contrast and facilitate single-cell imaging ([16]).

Although the flow cytometry analysis showed that the SPIO particles did not affect the physical maturation of DCs, we were interested in understanding how much iron from the SPIO particles was present in the cell and whether it had any potential effect on their intracellular organelles. Therefore, we measured the concentration of iron by inductively coupled plasma–mass spectrometry and developed an analysis program to calculate the surface area occupied by the particles in the cell. On average, the clusters of SPIO particles in the endocytic vesicles accounted for little of the surface area. Quantitative analysis from our study showed that the SPIO particles occupy approximately 0.35% of the total surface area in DCs (Fig. 5), and the total iron content is equivalent to 34.6 pg iron/cell.

To explore the detection threshold of 4.7-T MR on the migration of labeled DCs, we injected either 4000 or 1.0×10^6 labeled cells (30 μL each) into the left or right foot pad. Our study demonstrated that it is possible to track the migration of a small population of DCs, using the optical technique developed from our group ([8]) for guidance on the kinetics of cell migration. This work revealed that the optimal time for obtaining an ideal signal after injection of the labeled DCs in the foot pad was 24 h. Pre- and postcontrast from Fig. 6 shows that after 24 h, the DCs have indeed migrated from the injection site to the corresponding popliteal LN, resulting in a significant reduction in the T_2-mediated signal intensity. Quantitatively, the mean signal intensity postcontrast was significantly decreased, from 133 ± 17.9 to 27.4 ± 23.3 ($P < 0.005$), and 121 ± 13.7 to 53.5 ± 11.2 ($P < 0.002$) for the right and left popliteal LNs, respectively. The physical migration of DCs into the popliteal LNs caused an increase in the overall dimension from half to double the original size, depending on the number of cells injected. Quantitative measurement of the number of DCs that migrated from the injection site into the popliteal LNs was achieved by determining the iron concentration using inductively coupled plasma–mass spectrometry against the LNs of untreated animals on account of the intrinsic iron. The results were similar to our previous observation that only a portion of injected DCs could migrate to the first LNs ([8]). Our observation is inconsistent with others that the number of migration cells can vary from 0.7–5% ([17]).

We did not, however, observe any further DC migration from one LN to the next. At 24 h postinjection, we scanned for popliteal and inguinal LNs. There was an apparent change in the signal intensity of the former, but no equivalent effect was observed for the latter. Even though the right LN swelled to more than double its original size, there was no evidence that the DCs attempted to escape to another LN in this saturated environment. After MRI, animals were sacrificed and the iron concentration was determined from isolated LNs using inductively coupled plasma–mass spectrometry. The iron level in the treated inguinal LNs was equivalent to that of the control untreated counterparts. This observation demonstrated that injection of DCs into the foot pad guaranteed homing into the popliteal LN. Furthermore, once the DCs home in the draining LN, it is likely that they do not migrate to the neighboring LNs. It would be very interesting for future studies to compare the effects of SPIO labeling on migration of the DCs. Will the gravity caused by the mass uptake of SPIO particles affect the buoyancy of the DCs? Immunohistology and iron staining of the popliteal LN from an animal injected with SPIO-DCs through the foot pad compared to the other side of the same animal reveal an intense infiltration of the DCs beyond the intrinsic residential DCs, which is consistent with the MRI data (Fig. 7). We have consistently observed among multiple samples that the majority of the cells migrated to the cortex of the LNs within 24 h postinjection, with some cells proceeding to the paracortex zone.

CONCLUSION

The results of our study demonstrate that it is feasible to use this newly developed SPIO particle technology to track the migration of DCs using MRI. On their own, the cells can independently uptake SPIO particles, but at a retarded rate, whereas PL treatment facilitates particle internalization with remarkable efficiency. Furthermore, when using the transfecting reagent, we showed that it is possible to track the migration of as few as 4000 injected DCs.

In addition to the potential benefit of a direct translational application of our findings for clinical studies using MRI and SPIO-labeled DCs, this study may also encourage further research into the mechanism of recruitment and entrapment of activated DCs in draining lymphoid tissues, an element considered a key criterion for successful immunotherapy. Currently, we are developing a novel chemistry for surface modification, with the aim of fabricating the particles with variety of functional groups. This will allow future bioconjugation and will support the multimodal imaging of DCs. The other potential use of the functionalized SPIO is to fabricate tumor antigens on the surface for inducing direct DC uptake in vivo. This approach has just demonstrated feasibility of tracking and quantifying DC scavenging of SPIO-tumor adjuvant using MRI ([18]).

Acknowledgments

This work is support by a grant from NIA (AG026366-01A1) and the developmental fund from the Department of Radiology to W.P. We acknowledge excellent help from Pamela Wirth with histology work.

References

1. Larsson M, Majeed M, Ernst JD, Magnusson KE, Stendahl O, Forsum U. Role of annexins in endocytosis of antigens in immature human dendritic cells. Immunology. 1997; 92:501–511. [PubMed: 9497492]

2. Mohty M, Olive D, Gaugler B. Leukemic dendritic cells: potential for therapy and insights towards immune escape by leukemic blasts. Leukemia. 2002; 16:2197–2204. [PubMed: 12399962]
3. Ni K, O'Neill HC. The role of dendritic cells in T cell activation. Immunol Cell Biol. 1997; 75:223–230. [PubMed: 9243286]
4. Fernandez NC, Lozier A, Flament C, Ricciardi-Castagnoli P, Bellet D, Suter M, Perricaudet M, Tursz T, Maraskovsky E, Zitvogel L. Dendritic cells directly trigger NK cell functions: cross-talk relevant in innate anti-tumor immune responses in vivo. Nat Med. 1999; 5:405–411. [PubMed: 10202929]
5. Yang L, Carbone DP. Tumor-host immune interactions and dendritic cell dysfunction. Adv Cancer Res. 2004; 92:13–27. [PubMed: 15530555]
6. Barratt-Boyes SM, Watkins SC, Finn OJ. In vivo migration of dendritic cells differentiated in vitro: a chimpanzee model. J Immunol. 1997; 158:4543–4547. [PubMed: 9144465]
7. Prince HM, Wall DM, Ritchie D, Honemann D, Harrrison S, Quach H, Thompson M, Hicks R, Lau E, Davison J, Loudovaris M, Moloney J, Loveland B, Bartholeyns J, Katsifis A, Mileshkin L. In vivo tracking of dendritic cells in patients with multiple myeloma. J Immunother. 2008; 31:166–179. [PubMed: 18481386]
8. Pham W, Xie J, Gore JC. Tracking the migration of dendritic cells by in vivo optical imaging. Neoplasia. 2007; 9:1130–1137. [PubMed: 18084620]
9. Ahrens ET, Feili-Hariri M, Xu H, Genove G, Morel PA. Receptor-mediated endocytosis of iron-oxide particles provides efficient labeling of dendritic cells for in vivo MR imaging. Magn Reson Med. 2003; 49:1006–1013. [PubMed: 12768577]
10. de Vries IJ, Lesterhuis WJ, Barentsz JO, Verdijk P, van Krieken JH, Boerman OC, Oyen WJ, Bonenkamp JJ, Boezeman JB, Adema GJ, Bulte JW, Scheenen TW, Punt CJ, Heerschap A, Figdor CG. Magnetic resonance tracking of dendritic cells in melanoma patients for monitoring of cellular therapy. Nat Biotechnol. 2005; 23:1407–1413. [PubMed: 16258544]
11. Mowat P, Franconi F, Chapon C, Lemaire L, Dorat J, Hindre F, Benoit JP, Richomme P, Le Jeune JJ. Evaluating SPIO-labelled cell MR efficiency by three-dimensional quantitative T2* MRI. NMR Biomed. 2007; 20:21–27. [PubMed: 16998951]
12. Woo K, Hong J. Surface modification of hydrophobic iron oxide nanoparticles for clinical applications. IEEE Trans Magn. 2005; 41:4137–4139.
13. Inaba K, Inaba M, Romani N, Aya H, Deguchi M, Ikehara S, Muramatsu S, Steinman RM. Generation of large numbers of dendritic cells from mouse bone marrow cultures supplemented with granulocyte/macrophage colony-stimulating factor. J Exp Med. 1992; 176:1693–1702. [PubMed: 1460426]
14. Carson, FL. Histotechnology, a self-instructional text. Chicago: ASCP press; 1990. Prussian blue staining for ferric iron; p. 214-215.
15. Baumjohann D, Hess A, Budinsky L, Brune K, Schuler G, Lutz MB. In vivo magnetic resonance imaging of dendritic cell migration into the draining lymph nodes of mice. Eur J Immunol. 2006; 36:2544–2555. [PubMed: 16909432]
16. Dodd SJ, Williams M, Suhan JP, Williams DS, Koretsky AP, Ho C. Detection of single mammalian cells by high-resolution magnetic resonance imaging. Biophys J. 1999; 76(1 pt 1):103–109. [PubMed: 9876127]
17. MartIn-Fontecha A, Sebastiani S, Hopken UE, Uguccioni M, Lipp M, Lanzavecchia A, Sallusto F. Regulation of dendritic cell migration to the draining lymph node: impact on T lymphocyte traffic and priming. J Exp Med. 2003; 198:615–621. [PubMed: 12925677]
18. Long CM, van Laarhoven HW, Bulte JW, Levitsky HI. Magnetovaccination as a novel method to assess and quantify dendritic cell tumor antigen capture and delivery to lymph nodes. Cancer Res. 2009; 69:3180–3187. [PubMed: 19276358]

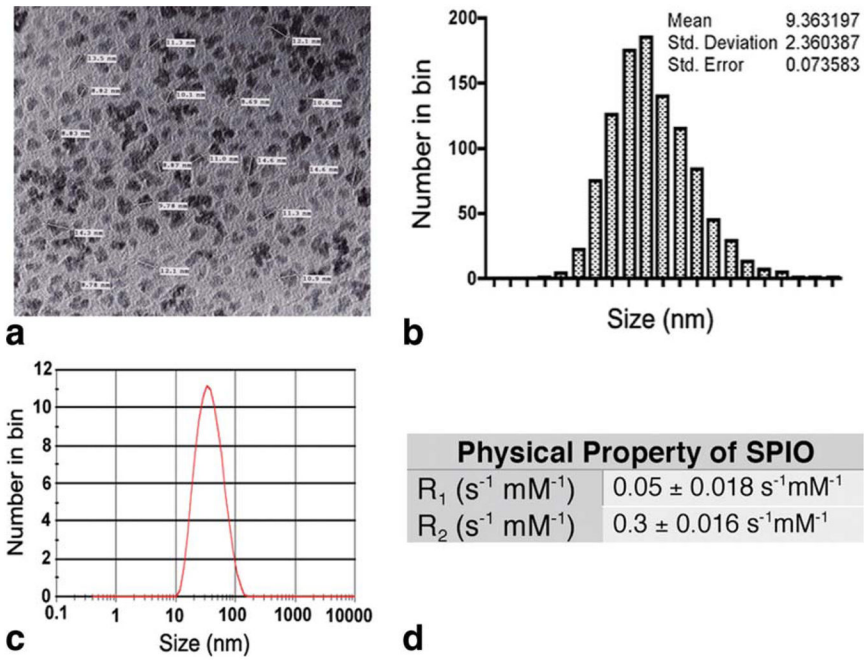

FIG. 1.

Physical properties of the synthesized dextran-coated SPIO particles. **a:** TEM image of the SPIO nanoparticles. **b:** The distribution of the iron core calculated from the TEM image. **c:** The overall size of dextran-coated SPIO particles was measured by a Zetasizer. **d:** The *R* values.

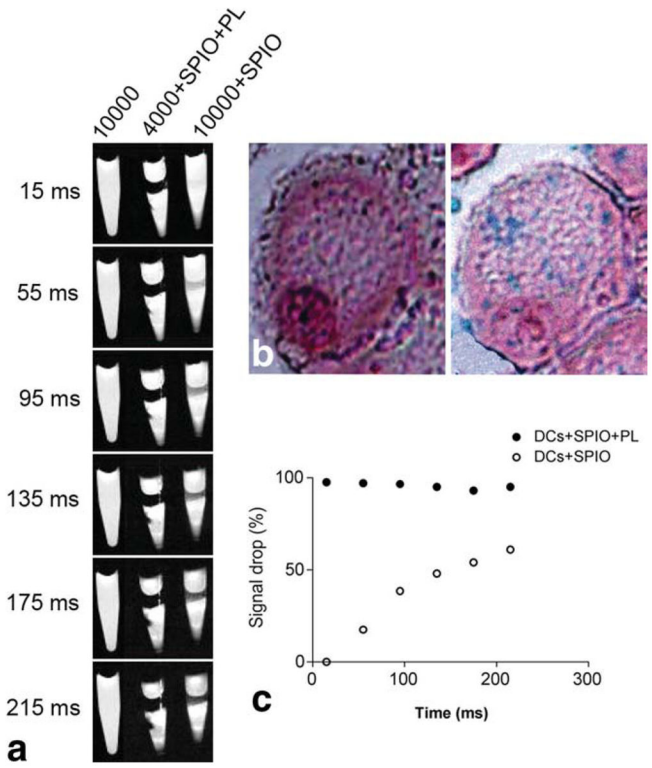

FIG. 2.

a: Magnetic resonance imaging of gelatin-embedded DCs at 4.7 T after incubation with SPIO for 1 h, with or without PL. The density of cells is represented by the numbers. **b:** Visualization using Prussian blue staining of the internalized SPIO particles with (right) and without (left) the presence of PL. **c:** Quantification of the signal drop caused by the presence of SPIO in the gelatin phantom tube as a percentage compared to the control.

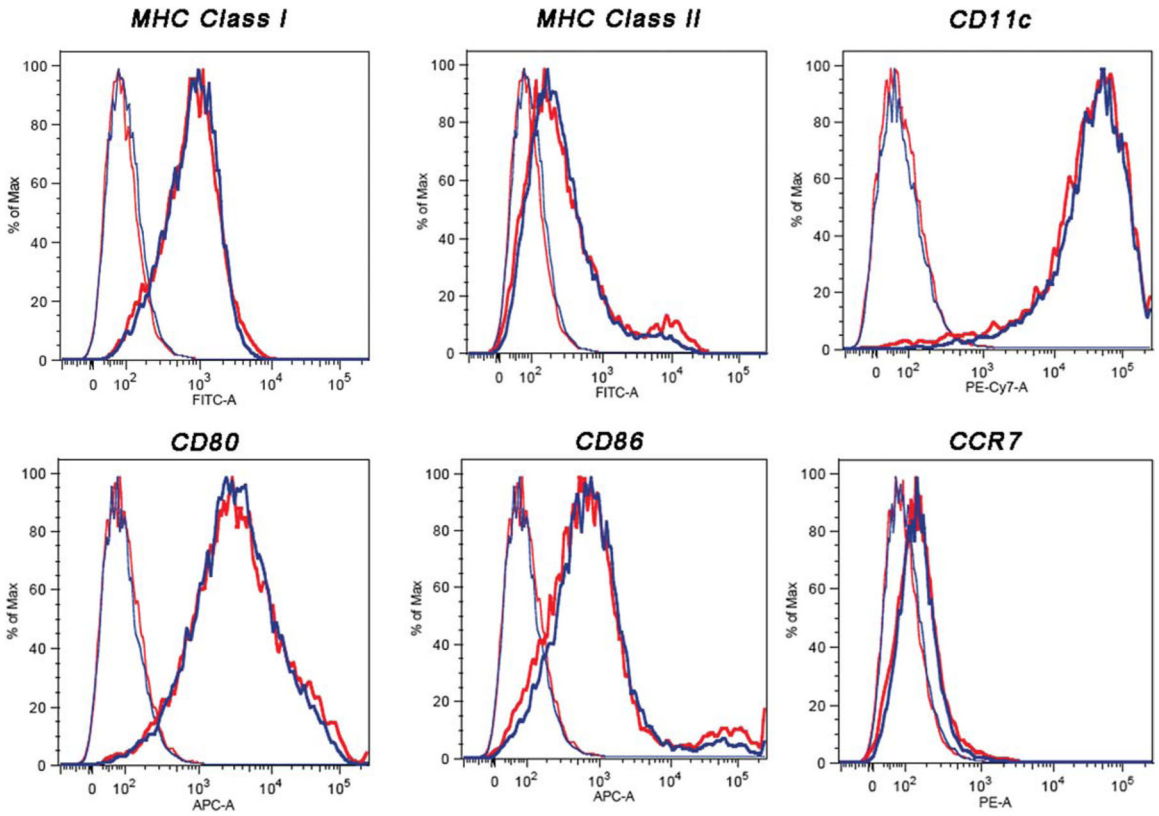

FIG. 3.

Cell surface phenotype as determined by flow cytometry of unlabeled (blue) and SPIO-labeled (red) murine-derived DCs. After 1 h of incubation with SPIO in the presence of PL, cells were stained with phycoerythrin-conjugated monoclonal antibodies for CD11c, presentation receptors MHC-I and MHC-II, costimulatory receptors CD80 and CD86, and chemokine receptors CCR7. The left histograms represent unstained labeled and unlabeled cells as controls. The shifted histograms represent stained labeled and unlabeled DCs. The y-axis of each histogram shows the relative cell number; the x-axis shows the log fluorescence intensity.

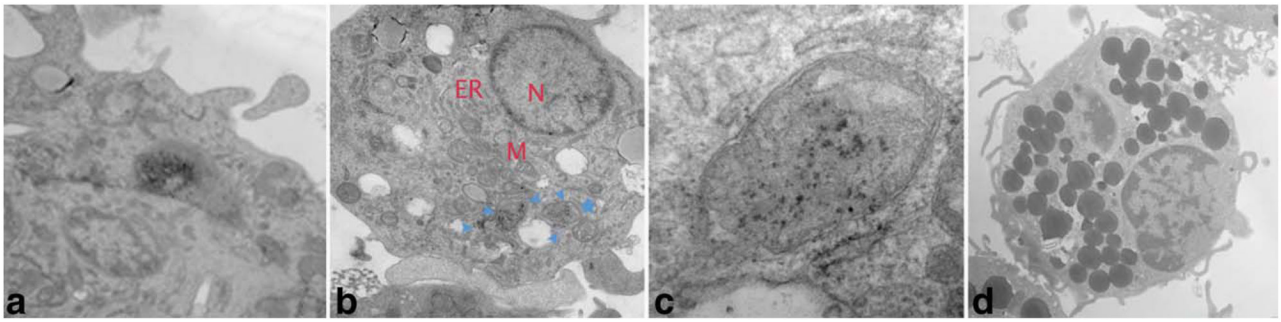

FIG. 4.

Morphologic analysis of labeled DCs. Cells were incubated with SPIO for 1 h in the presence of PL and then processed for TEM analysis. **a:** Initial point of entry after membrane association; **(b)** SPIO-containing vesicles in the cytoplasm (arrowheads); **(c)** enlarged vesicle in b (star), and **(d)** control DCs without SPIO.

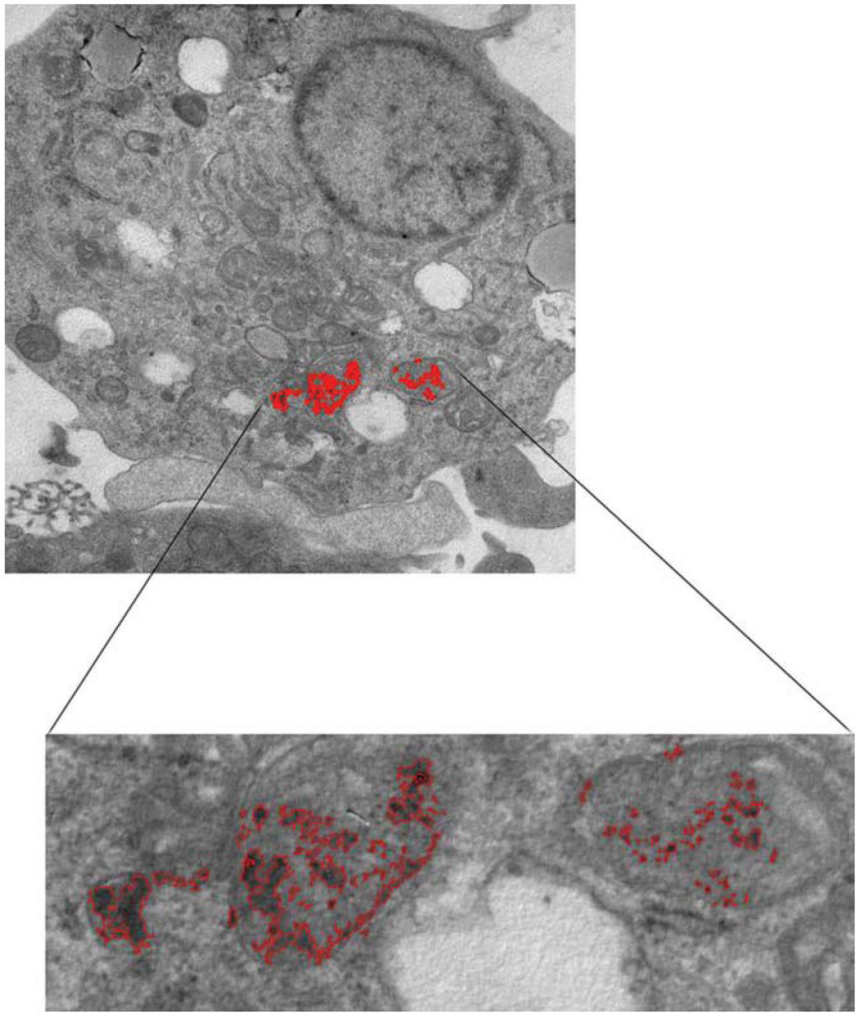

FIG. 5.

Surface area occupancy of SPIO in a DC was calculated using a program written in house with MATLAB. SPIO vesicles occupy ~0.35% of cell space.

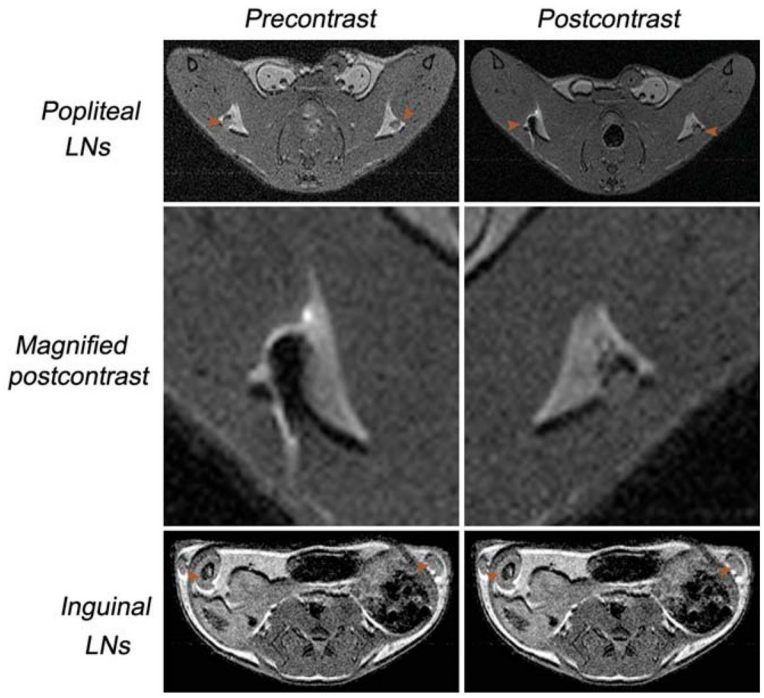

FIG. 6.

Transaxial in vivo multispin-echo MRIs (TE = 10 ms, TR = 2–3 sec) of mice before and after distribution of the labeled cells via the foot pad. The LNs are indicated by arrows. The signal intensity of the popliteal LNs appears darker, suggesting the migration and homing of the DCs. No signal intensity change was detected before or after injection of SPIO-labeled DCs in inguinal LNs.

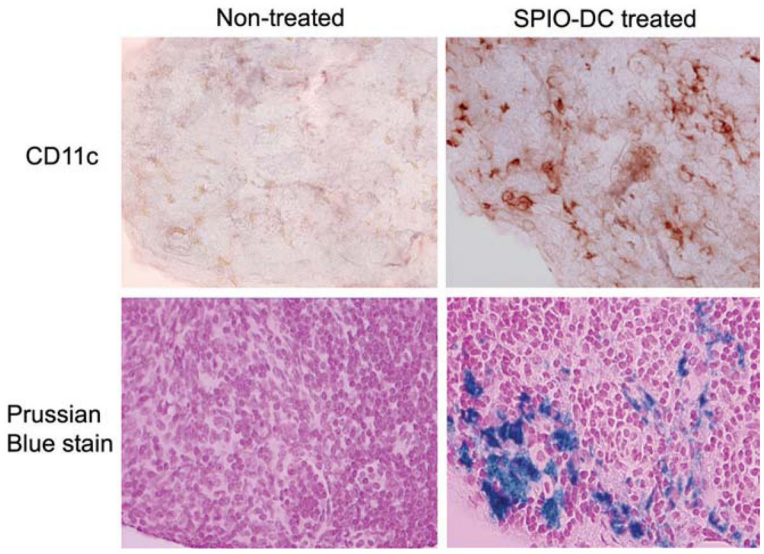

FIG. 7.

Immunohistochemical and iron staining (both ×40) of consecutive tissue slides of the popliteal LNs, either untreated or treated, with foot pad injection of SPIO-DCs over the course of 24 h.